

## Folding Simulations of the Transmembrane Helix of Virus Protein U in an Implicit Membrane Model

Jakob P. Ulmschneider<sup>\*,†</sup> and Martin B. Ulmschneider<sup>‡</sup>

*Department of Chemistry, University of Rome “La Sapienza”, Rome, Italy, and  
Department of Biochemistry, University of Oxford, Oxford, U.K.*

Received May 2, 2007

**Abstract:** Vpu is an 81-amino-acid auxiliary membrane protein encoded by human immunodeficiency virus type 1 (HIV-1). One of its roles is to amplify viral release by self-assembling in homo-oligomers to form functional water-filled pores enabling the flux of ions across the membrane. Various NMR and CD studies have shown that the transmembrane domain of Vpu has a helical conformation. With a recently developed implicit membrane model and an efficient Monte Carlo (MC) algorithm using concerted backbone rotations, we simulate the folding of the transmembrane domain of Vpu at atomic resolution. The implicit membrane environment is based on the generalized Born theory and enables very long time scale events, such as folding to be observed using detailed all-atom representation of the protein. Such studies are currently computationally unfeasible with fully explicit lipid bilayer molecular dynamics simulations. The correct helical transmembrane structure of Vpu is predicted from extended conformations and remains stably inserted. Tilt and kink angles agree well with experimental estimates from NMR measurements. The experimentally observed change in tilt angle in membranes of varying hydrophobic width is accurately reproduced. The extensive simulation of a pentamer of the Vpu transmembrane domain in the implicit membrane gives results similar to the ones reported previously for fully explicit bilayer simulations.

### Introduction

One of the most interesting challenges of theoretical biophysics is the direct computational prediction of membrane protein structure from sequence information. Unfortunately, molecular mechanics simulations using explicit lipid-bilayer membranes<sup>1–4</sup> are usually limited to the 1–100 ns time scale due to the large number of nonbonded interactions that need to be evaluated for such complex systems. While this allows for the study of protein stability in a lipid bilayer<sup>1,2</sup> or even self-assembly of protein/detergent micelles for various proteins,<sup>5,6</sup> it is unfortunately inadequate to study protein folding, which requires time scales in the micro- to millisecond range. In principle folding can be simulated for tiny systems in explicit lipid bilayer membranes when very large

computational resources are available, e.g., 64 CPUs for 2.6 ns replica exchange molecular dynamics of a 16 residue peptide in a 36 lipid bilayer solvated by 1048 water molecules.<sup>4</sup> Nevertheless, even this approach is currently unfeasible for larger systems or for studies of protein function. Simulations in the multi- $\mu$ s range for molecular dynamics (MD) or in the billions of Monte Carlo (MC) steps are needed to study folding and to obtain converged averages of experimentally measurable macroscopic properties. A further overview on the large number of present and anticipated future applications of implicit membrane methods is given in recent reviews.<sup>7–9</sup>

Implicit solvation models generally treat the solvent as a polarizable continuum. For spherical ions in a homogeneous isotropic dielectric the solvation energy can be determined analytically as demonstrated by Born.<sup>10</sup> The generalized Born solvation model extends this equation to macromolecules, which are approximated as an assortment of charged

\* Corresponding author e-mail: Jakob@ulmschneider.com.

<sup>†</sup> University of Rome “La Sapienza”.

<sup>‡</sup> University of Oxford.

spheres.<sup>11</sup> The immense success of this method in globular protein and peptide folding simulations<sup>12–16</sup> has encouraged attempts to apply the generalized Born formalism to represent the membrane environment implicitly.<sup>17–27</sup> These models describe the membrane environment as a uniform hydrophobic slab and have been used successfully to fold and assemble small helical membrane peptides.<sup>18,23,24</sup> The combination with sophisticated Monte Carlo methods has enabled us to successfully study the folding and orienting of membrane associated peptides into their experimentally observed native conformations.<sup>21,27</sup>

In this study, we report folding simulations of Virus protein U (Vpu), a 81-residue membrane protein of the human immunodeficiency virus type 1 (HIV-1).<sup>28,29</sup> It consists of one N-terminal hydrophobic membrane helix and two shorter amphipathic helices that remain in the plane of the membrane on the cytoplasmic side.<sup>30</sup> Two main functions of Vpu are observed: The first, which involves the cytoplasmic domain in the C-terminal half of the protein, is to accelerate the degradation of the CD4 receptor in the endoplasmic reticulum (ER) of infected cells.<sup>31,32</sup> Second, Vpu has been shown to amplify the release of virus particles from infected cells, a process that involves the transmembrane (TM) domain.<sup>33,34</sup> Vpu and its isolated TM part oligomerize in lipid membranes<sup>35</sup> and show channel activity.<sup>36–40</sup> In this work, we focus on the TM  $\alpha$ -helix of Vpu: Its structure has been determined experimentally,<sup>41</sup> and its orientation relative to the plane of the lipid bilayer has been estimated from both NMR spectroscopy<sup>41–44</sup> and Fourier Transform Infrared Dichroism (FTIR) spectroscopy.<sup>45</sup>

Several previous MD simulation studies have been performed on Vpu in explicit bilayers, with either the complete peptide,<sup>46</sup> part of the peptide,<sup>47,48</sup> or only the N-terminal TM helix as monomer or as oligomer.<sup>49–55</sup> However, the short time scale ( $\sim 1–5$  ns) of these simulations was not sufficient to study folding or function. Longer simulations (200 ns) of Vpu have been performed using a coarse-grain method.<sup>56</sup> In this work, we use our implicit membrane model together with a MC scheme to simulate the folding of the TM helix of Vpu as well as study its oligomeric structure in the membrane.

## Simulation Methods

**The Generalized Born Membrane.** The development of the present generalized Born (GB) membrane has been described in detail in a previous publication.<sup>21</sup> The GB equation<sup>11</sup> is left unchanged, and only the method to calculate the Born radii is modified. The total effective free energy of solvation in the membrane is given by  $\Delta G_{\text{sol}} = \Delta G_{\text{pol}} + \Delta G_{\text{np}}$ , where  $\Delta G_{\text{pol}}$  is the electrostatic contribution (GB equation)

$$\Delta G_{\text{pol}} = -166 \left( \frac{1}{\epsilon_m} - \frac{1}{\epsilon_w} \right) \sum_i^n \sum_j^n \frac{q_i q_j}{\sqrt{r_{ij}^2 + \alpha_j \alpha_i \exp(-r_{ij}^2/4\alpha_i \alpha_j)}} \quad (1)$$

and  $\Delta G_{\text{np}}$  is the nonpolar hydrophobic contribution. The membrane is treated as a planar hydrophobic region in a

uniform polar solvent with a dielectric constant  $\epsilon_w = 80$ , that becomes increasingly inaccessible to the solvent toward its center.

Both the protein interior and the membrane are assumed to have the same interior dielectric constant of  $\epsilon_m = 2$ . The Born radii are calculated using the fast asymptotic pairwise summation of Qiu and Still,<sup>57</sup> where the integral of  $1/r^4$  over the solute interior is approximated as a sum

$$G'_{\text{pol},i} = \Gamma(z_i, R_i, L) + \underbrace{\sum_j^{1-2} \frac{P_2 V_j(z_j)}{r_{ij}^4} + \sum_j^{1-3} \frac{P_3 V_j(z_j)}{r_{ij}^4} + \sum_j^{1 \geq 4} \frac{P_4 V_j(z_j) \text{ ccf}}{r_{ij}^4}}_{\text{sums only involving atoms with } |\lambda| > L}, \quad (2)$$

where  $L$  is the membrane half width,  $z_i$  is the  $z$ -position of the atom  $i$ ,  $P_1–P_4$  are the parameters determined by Qiu et al.,<sup>57</sup> the sums are over 1–2, 1–3, and  $1 \geq 4$  neighbors and  $\text{ccf}$  is a close contact function, and  $V_i(z)$  is the volume of atom  $i$ . The main advantage of the asymptotic approach over other methods to obtain Born radii is speed: Pairwise evaluation of the costly  $1/r_{ij}$  terms already occurs for the nonbonded Coulomb and van der Waals interactions. In our program, the calculation of the Born radii  $1/r_{ij}^4$  terms in eq 2 is combined with the other nonbonded calculations. As a result, the evaluation of the Born radii (through eq 2) takes no additional computational time, i.e., is obtained ‘for free’. The increase in computation is entirely due to the evaluation of eq 1 and results in a slowdown of  $\sim 2.0–2.2$  compared to vacuum simulations. This is at the lower end of the values reported for other GB models, which usually are in the range  $\sim 4–5$ .<sup>58,59</sup> In addition to the good performance, the method has been demonstrated to yield excellent results in predicting experimental free energies of solvation as well as hydration effects on conformational equilibria.<sup>60</sup>

By modifying the pairwise summation to solute atoms, the self-solvation terms  $\Gamma(z_i, L)$  as well as the atomic volumes  $V(z_i)$  were made to vary smoothly between full solvation and a limiting value for burial at the center of the membrane. We use a Gaussian shape

$$\Gamma(z_i) = g_{\text{bulk}} + (g_{\text{center}} - g_{\text{bulk}}) e^{\gamma(z_i^2/L^2)} \quad (3)$$

where  $g_{\text{bulk}}$  is the limiting value of  $\Gamma$  at a large distance from the membrane (i.e.,  $z \gg L$ ) corresponding to the self-solvation term of the unmodified generalized Born method  $g_{\text{bulk}} = -166/(R_i + \text{offset} + P_1)$ , while  $g_{\text{center}}$  is the value of  $\Gamma$  at the membrane center. We used a Gaussian with  $\gamma = -2.0$  and a membrane half width of  $L = 15 \text{ \AA}$ , while  $g_{\text{center}} = -7.67 \text{ kcal/mol}$ , as reported previously.<sup>17,21,61</sup>

The nonpolar part of the solvation free energy  $\Delta G_{\text{np}}$  is modeled using an effective surface tension associated with the solvent accessible surface area.<sup>57</sup> Instead of a costly calculation of the accurate surface area, a mimic based on the Born radii is used, which has been shown to be very accurate but much faster.<sup>62</sup> As it is moved toward the center of the membrane the surface energy contribution of each atom is scaled down by a Gaussian function of the same width as  $\Gamma$ . For distances far from the membrane (i.e.,  $z \gg$

*L*) the nonpolar contribution is included with the positive surface tension of solvation in water, while in the center of the membrane the surface tension is negative (i.e., energy is gained by moving into this phase from the gas phase) as determined experimentally.<sup>63</sup> The surface tension contribution of each atom was varied using a Gaussian function with  $\gamma = -1.5$ , interpolating between the limiting values of 12 cal/mol·Å<sup>2</sup> in bulk solvent and  $-19$  cal/mol·Å<sup>2</sup> at the membrane center.

The present membrane model neglects any effects due to differences in lipid composition, density, and charge distribution of the two bilayer leaflets as well as effects due to the transmembrane voltage. However, it is in principle possible to include these properties by replacing the Gaussians with an equivalent nonsymmetric function. The nonpolar part of the implicit membrane model was previously parametrized against experimental transfer free energies of hydrophobic side-chain analogs,<sup>63</sup> and no parameters were optimized for the present simulations.

**Monte Carlo Sampling.** The implicit membrane model has been implemented as part of an all-atom Monte Carlo program. An efficient concerted rotation sampling technique<sup>64</sup> is used to move the protein backbone; in addition there are single rapid side-chain moves, with a ratio of 3 side-chain moves per backbone move. The potential energy is evaluated with the OPLS all-atom force field.<sup>65</sup> All nonbonded interactions as well as the GB energy are truncated using a residue-based cutoff of 14 Å, but no cutoffs are used in the pentamer simulation. In addition, one folding simulation is run without cutoff to compare to the run using cutoffs. The Born radii are recomputed for every configuration. The described setup has been shown to perform well in sampling DNA<sup>66</sup> and protein folding simulations.<sup>16</sup> We have recently demonstrated that this method is equivalent to molecular dynamics sampling, with both methods able to find the native state of several polypeptides with comparable computational effort.<sup>67</sup>

**Replica Exchange MC (REMC).** The replica exchange method has recently been reviewed in detail.<sup>68,69</sup> Ten replicas of each system were set up with identical fully extended initial configuration and exponentially spaced temperatures in the range 300–500 K. Every 10<sup>4</sup> Monte Carlo moves a replica swap with transition probability

$$p_{1 \rightarrow 2} = \exp(-\Delta) \quad (4)$$

where

$$\Delta = \left( \frac{1}{kT_1} - \frac{1}{kT_2} \right) (E_1 - E_2) \quad (5)$$

is attempted.  $E_1$  and  $E_2$  are the total energies of two conformers at temperatures  $T_1$  and  $T_2$ , respectively. High-temperature replicas facilitate the crossing of energy barriers, while low-temperature replicas extensively sample low-energy conformations. This enables the efficient and increased sampling of the entire system by frequent crossing of high-energy barriers. The exponential temperature spacing ensures a constant acceptance rate of all adjacent replica swaps.<sup>68</sup>

**Vpu.** The 30-residue TM domain of Vpu was set up identical to the NMR experiments (PDB code 1pje)<sup>41</sup> and has the sequence MQPIQIAIVALVVVAIIIVVWSIVIIEGR. An additional six-residue “solubility tag” at the C terminus used in the experiments is omitted in the simulations. The experiments did not locate all residues present in the peptide. The missing residues (1–6, 26–30) are the polar and charged residues at the helix termini, which are important for the correct orientation of the helix in the membrane. To be able to compare the current analysis with the experiment, the missing residues were added with optimized geometry in an  $\alpha$ -helical secondary structure for the pentamer simulations. The Vpu TM monomer folding simulations were started from completely extended conformation arranged so that they span the membrane.

**Free Energy Analysis.** The free-energy was calculated as a function of the helix tilt and center-of-mass position along the membrane normal. For a system in thermodynamic equilibrium, the change in free energy on going from one state to another is given by

$$\Delta G = -RT \ln \frac{p_1}{p_2} \quad (6)$$

where  $R$  is the ideal gas constant,  $T$  is the temperature, and  $p_i$  is the probability of finding the system in state  $i$ . The free energy is plotted on a two-dimensional grid, and the values are shifted so that the lowest bin is zero.

**Rigid Body Energy Scan.** The minimal energy conformation was calculated by exploring the entire translational and rotational space of a completely helical rigid structure of VPU in the membrane. The principal axis of the protein was determined through diagonalization of the inertia tensor using only the heavy backbone atoms. The tilt angle was defined as the angle of the principal axis with respect to the membrane normal, while the rotation angle was defined as the angle of rotation around the principal axis.

The helix was translated from  $-50$  Å to  $+50$  Å along the membrane normal (membrane center = 0 Å) in 1 Å steps. At each step the protein was rotated through all space to find the orientation of minimum energy by first tilting it with respect to the membrane normal and subsequent rotation around its principal axis until all tilt and rotational states have been sampled with a step size of 5°. The lowest energy conformation encountered was then subjected to a rigid body minimization in order to locate the precise location of the global energy minimum.

## Results

**Insertion Energy Landscape.** In order to investigate the insertion-energy landscape for the local minimum energy orientations the implicit membrane potential was plotted as a function of position along the membrane normal and tilt angle, while the rotation angle was optimized (i.e., the rotation angle for each position and tilt angle is such that the energy is minimal). Figure 1 panel C shows the resulting insertion energy landscape for a completely helical structure of Vpu. The zero point of the potential was chosen at an infinite distance from the membrane. Vpu has four distinct

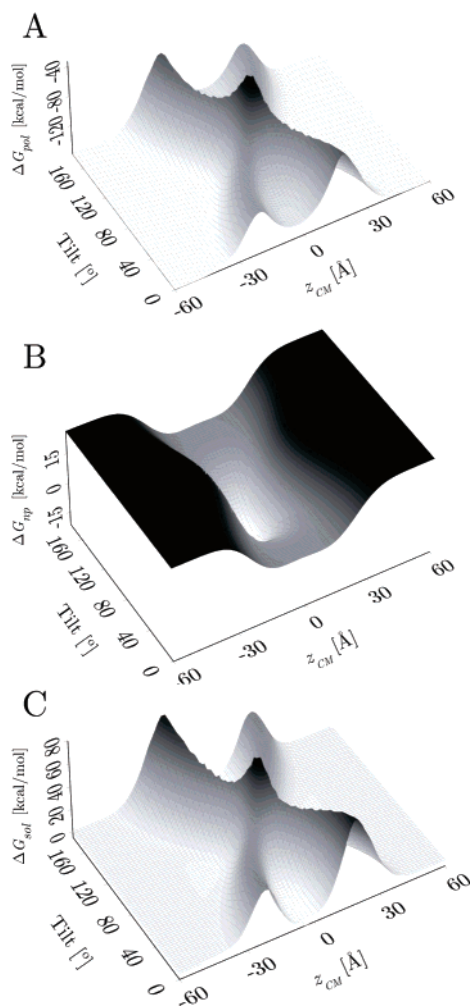


**Figure 1.** Insertion energy profiles. The figure shows the insertion energy of the Vpu helix with charged termini as a function of the helix tilt and center-of-mass position along the membrane normal for the optimized rotation angle (around the long axis of the helix). Panel A shows the polarization energy, panel B nonpolar energy, and panel C the total solvation energy, shifted such that it is zero at an infinite distance from the membrane.

minima, the two deepest corresponding to inserted configurations with the helices approximately parallel to the membrane normal. The other two minima are surface bound configurations with the helix axis parallel to the plane of the membrane. It should be noted that due to the symmetry of the membrane model, the cytoplasmic and intracellular minima have identical insertion energies, as do the two inserted minima.

Generally the inserted TM configuration corresponds to the global energy minimum. The insertion energy is  $-5.5$  kcal/mol, with a tilt angle of  $5.6^\circ$  as well as position close to the center of the membrane—slightly shifted to  $3.7$  Å. Adsorption of the peptide onto the membrane surface is also favorable but to a significant lesser extent, with an energy minimum of  $-0.8$  kcal/mol at  $20$  Å, and a parallel orientation with tilt angle of  $80^\circ$ .

To investigate the relative roles of the polar and nonpolar part of the implicit membrane energy, their contributions to the total insertion potential was also calculated. Figure 1

shows the contributions of  $\Delta G_{\text{pol}}$  (panel A) and  $\Delta G_{\text{np}}$  (panel B) to the overall insertion-energy landscape (panel C). Burial of charged and polar residues in the membrane interior is highly unfavorable, and the characteristic ‘X’ shape of  $\Delta G_{\text{pol}}$  is caused by the position of such residues at the helix termini.<sup>70,71</sup> The hydrophobic effects are the main contributors to helix insertion and, as expected, give the lowest contribution for a completely buried helix parallel and in the center of the membrane (panel B). It is generally recognized that overall hydrophobicity is the main driving force for the integration of TM helices into the lipid bilayer.<sup>72</sup> Indeed the vast majority of residues in TM helices are hydrophobic.<sup>73</sup> Nevertheless, polar, charged, and aromatic residues are known to be important for anchoring the helix termini into the lipid headgroup environment at the membrane interfaces.<sup>74–76</sup> The overall potential favors TM orientations since hydrophobic residues strongly prefer an inserted to a surface-bound configuration. For the burial of a typical TM peptide of about 20 residues in the membrane, White et al. roughly estimate a hydrophobic contribution of  $\sim 40$  kcal/mol, offsetting a unfavorable dehydration of the  $\alpha$ -helical peptide backbone of about  $\sim 30$  kcal/mol. This results in a net favorable free energy of about  $\sim 10$  kcal/mol.<sup>77</sup> From the orientational scan of Vpu, we estimate a hydrophobic contribution of  $-22.5$  kcal/mol and a polarization penalty of  $+17$  kcal/mol, resulting in the  $-5.5$  kcal/mol insertion of the TM helix with respect to a helix in solution.

**Role of Terminal Charges.** When calculating the properties of membrane proteins, it is important to take into account the charge state of the amino acid side chains. The implicit membrane model is very sensitive to changes in charge since burial of charged groups is highly unfavorable. For Vpu, both Glu 28 and Arg 30 are modeled in their charged state (pH = 7). In addition, the chain ends can be modeled as either charged ( $\text{NH}_3^+/\text{COO}^-$ ) or capped with methyl groups, neutralizing the termini. The lack or presence of this additional dipole has a strong effect on the outcome of the simulations: in the capped case, there is no strongly charged group on the N-terminal part of the peptide. This has a significant effect on the insertion energy landscape discussed above. Figure 3 shows  $\Delta G_{\text{pol}}$  recalculated for the capped system, revealing a markedly different shape than the uncapped system given in Figure 1 panel C. The lack of a charged residue on the N-terminal side of the helix results in a considerable lowering of the barrier ( $\sim 6$  kcal/mol) on the N-terminal side of the transmembrane inserted minimum. The characteristic ‘X’ shape is lost. While the peptide remains in a TM inserted conformation, the system can ultimately overcome the barrier and exit the membrane.

The experimental setup does not use an N-terminal cap but adds an additional six-residue “solubility tag” at the C terminus that facilitates the isolation, purification, and sample preparation of the peptide.<sup>41</sup> We model Vpu without the tag but both with caps and without to reveal the differences and role the charge state has on the implicit membrane model.

**Helix Tilting.** It has been experimentally observed that membrane proteins avoid unfavorable exposure of their hydrophobic surface to a hydrophilic solvent by matching

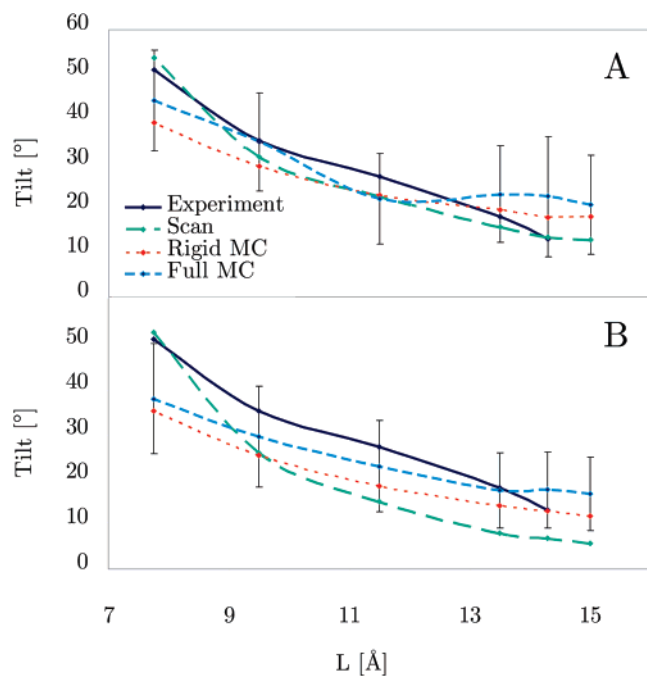


**Figure 2.** Tilt angle of Vpu as a function of the hydrophobic membrane half-width  $L$ , calculated for a  $\alpha$ -helical TM conformation. Panel A gives the results for the capped peptide, panel B for the system with uncapped chain ends. The tilt was calculated in three ways: The dashed line gives the tilt angle of the minima encountered in the rigid body scan. The dotted line shows the average tilt angles determined in a rigid body MC simulation ( $10^6$  MC steps) and the fine dashed line for a fully flexible MC simulation ( $10^9$  MC steps). In the MC simulations, the tilt angle fluctuates up to  $\pm 30^\circ$ , resulting in a large standard deviation of  $\sim 10^\circ$ , shown here as error bars for the full MC runs. There is little difference in the results of the capped and uncapped peptide, and in both cases the tilt angle obtained with the fully flexible simulations best matches the experimental values.

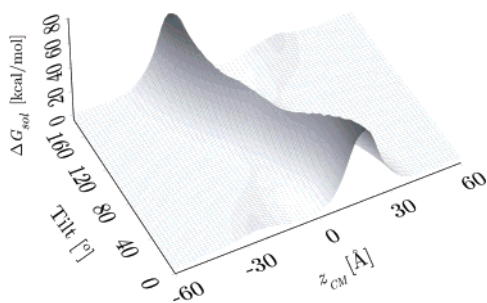


**Figure 3.** Insertion energy profile of the Vpu helix with capped uncharged termini as a function of the helix tilt and center-of-mass position along the membrane normal for optimized rotation angle (around the long axis of the helix). The lack of a charged residue on the N-terminal side of the helix results in a weak barrier ( $\sim 6$  kcal/mol) on one side of the transmembrane inserted minimum. This barrier is much larger in the uncapped helix (panel C of Figure 1).

the length of their hydrophobic helical segments to the thickness of the lipid bilayers ('hydrophobic mismatch').<sup>43,78–80</sup> Most easily, this occurs by structural adaptation such as changes in helix tilt and kink. Recently, the tilt angle of the

transmembrane segment of Vpu was determined experimentally in lipid bilayers of various thickness using solid-state NMR experiments of aligned samples<sup>43</sup> as well as bicelles.<sup>42</sup> These studies demonstrated that changes in tilt angle appear to be the principal mechanism for compensating the mismatch, with an increase from  $18^\circ$  for a hydrophobic width of  $2L = 27 \text{ \AA}$  to a much larger  $51^\circ$  for  $2L = 15.5 \text{ \AA}$ . In order to investigate this behavior with the implicit membrane model, a series of simulations was performed by adjusting the width of the hydrophobic segment,  $2L$ , reproducing the effect of the various lipid environments used in the experiments. For each membrane thickness, a complete translational and rotational scan (see method section) was performed with the perfectly  $\alpha$ -helical conformation found in the NMR measurements, in order to determine the tilt angle and  $z$ -position of the energy minimum. In the second stage, the helix was run in the membrane using a rigid-body MC simulation of  $1 \times 10^6$  MC steps length, giving the average values of the tilt and  $z$ . Finally, a third simulation was performed using a full MC run of the helix with complete flexibility for  $1 \times 10^9$  MC steps. Although computationally demanding, the full MC run corresponds most closely to the experimental setup, as the system can freely move, breathe, and reveal helix kinking or even unfolding. Thus, the averages here will be the most indicative of the quality of the model.

Due to the strong dependence of the results on the charge state of the terminal residues, all simulations were performed twice, for the capped peptide and the uncapped peptide. Table 1 shows the results for the case of the uncapped peptide. The experimental estimates of the membrane thickness and tilt angles were taken from the solid-state NMR measurements of Park et al. on phospholipids bilayers<sup>41,43</sup> and on bicelles.<sup>42</sup> For all simulations, the helix remains firmly inserted in the TM state, with a slight off-center position toward the N-terminus of  $2.9\text{--}4.5 \text{ \AA}$  and an insertion energy of  $\sim 5.5\text{--}8$  kcal/mol. The tilt angles are also plotted in Figure 2 panel A. There is overall good agreement with the experimental results, with the observed increase in tilt as the membrane width decreases. However, in a different experimental study of Vpu using infrared dichroism, the tilt angle was determined to be  $6.5^\circ \pm 1.7^\circ$ .<sup>45</sup> This is significantly lower than what we report here, and our values better fit the NMR data. There is a progressively better match as the simulation methodology becomes more thorough: the best results are obtained with the fully flexible MC simulations, revealing the importance of conformational flexibility in determining the configurational averages. The tilt angle fluctuates up to  $\pm 30^\circ$ , resulting in the large standard deviation of  $\sim 10^\circ$ , which could be due to the implicit nature of the membrane model. Thus the tilt cannot be calculated more accurately than  $\pm 10^\circ$ . The results for the capped Vpu are shown in Table 2 and plotted in Figure 2 panel B. Due to the low barrier, some of peptides in the long MC simulations exit the membrane after  $\sim 500 \times 10^6$  MC steps. For these data points, the averages are only over the TM part of the run.

The simulations all show strong kinking with angles of  $25\text{--}40^\circ$  at the center of the helix. However, no persistently

**Table 1.** Helix Tilt and z-Position of Uncapped Vpu<sup>a</sup>

<i>L</i> [Å]	exp. tilt [deg]	rigid scan (min)			rigid MC (10 <sup>6</sup> steps)		full MC (10 <sup>9</sup> steps)		
		<i>z</i> [Å]	tilt [deg]	Δ <i>G</i> [kcal/mol]	<i>z</i> [Å]	tilt [deg]	<i>z</i> [Å]	tilt [deg]	kink [deg]
15		3.8	5.7	−5.5	3.7 ± 1.5	11.8 ± 5.9	4.5 ± 2.1	16.6 ± 8.1	29.4 ± 12.6
14.3	13	3.8	6.8	−6.3	3.6 ± 1.5	12.9 ± 6.3	6.1 ± 2.0	17.5 ± 8.4	27.7 ± 11.4
13.5	18 (21)	3.7	7.9	−7.1	3.6 ± 1.5	14.0 ± 6.8	2.9 ± 2.1	17.5 ± 8.3	39.9 ± 17.1
11.5	27 (30)	3.9	14.9	−8.1	3.5 ± 1.6	18.3 ± 8.4	4.0 ± 2.5	22.8 ± 10.1	43.4 ± 15.3
9.5	35	3.5	25.8	−8.2	3.3 ± 2.1	25.1 ± 10.6	4.9 ± 2.7	29.4 ± 11.1	55.1 ± 16.4
7.75	51	4.3	52.5	−8.8	3.0 ± 2.7	34.9 ± 12.9	3.6 ± 3.3	37.7 ± 12.2	48.6 ± 16.4

<sup>a</sup> *L* is the membrane half width. The experimental helix tilt is taken from the solid-state NMR measurements of Park et al. on phospholipids bilayers<sup>43</sup> and on bicelles (brackets).<sup>42</sup> For the rigid body scan, the *z*-position and tilt of the minimum and its insertion energy with respect to infinite separation from the membrane is given. For the MC simulations, the averages of the *z*-position, tilt, and kink are given.

**Table 2.** Helix Tilt and z-Position of Capped Vpu<sup>a</sup>

<i>L</i> [Å]	exp. tilt [deg]	rigid scan (min)			rigid MC (10 <sup>6</sup> steps)		full MC (10 <sup>9</sup> steps)		
		<i>z</i> [Å]	tilt [deg]	Δ <i>G</i> [kcal/mol]	<i>z</i> [Å]	tilt [deg]	<i>z</i> [Å]	tilt [deg]	kink [deg]
15		5.0	12.8	−4.3	6.3 ± 2.3	18.1 ± 8.4	6.7 ± 2.3	20.8 ± 11.1	37.2 ± 10.6
14.3	13	4.4	13.4	−5.0	5.4 ± 2.2	17.8 ± 8.0	5.1 ± 3.4	22.5 ± 13.4	29.0 ± 12.0
13.5	18 (21)	4.3	15.6	−5.6	5.1 ± 2.6	19.5 ± 10.3	5.9 ± 2.4	23.1 ± 10.8	30.8 ± 12.6
11.5	27 (30)	3.9	22.6	−6.8	3.9 ± 2.0	22.8 ± 9.5	6.5 ± 2.3	22.0 ± 10.1	25.0 ± 11.2
9.5	35	3.5	31.5	−7.4	3.2 ± 2.3	29.3 ± 11.2	3.2 ± 2.5	34.8 ± 11.1	42.8 ± 12.2
7.75	51	4.5	53.7	−8.4	2.9 ± 2.6	39.1 ± 12.6	2.2 ± 2.7	44.1 ± 11.4	38.3 ± 14.5

<sup>a</sup> *L* is the membrane half width. The experimental helix tilt is taken from the solid-state NMR measurements of Park et al. on phospholipids bilayers<sup>43</sup> and on bicelles (brackets).<sup>42</sup> For the rigid body scan, the *z*-position and tilt of the minimum and its insertion energy with respect to infinite separation from the membrane is given. For the MC simulations, the averages of the *z*-position, tilt, and kink are given.

kinked structures are observed, with very fast fluctuation of the kink angle during the simulations. Interestingly, the kinking behavior is little influenced by either the membrane width or the charge state of the termini (see Tables 1 and 2). Experimentally, only a slight kink of 1–5° is observed at Ile 17 in both micelle and lipid mixture (9:1, DOPC:DOPG) bilayer environments,<sup>41</sup> but none is found in thinner bilayers<sup>43</sup> or in bicelles.<sup>42</sup> Simulations of Vpu oligomers with explicit lipid and solvent molecules have reported higher kink angles of 12.7–19.9°,<sup>52</sup> and in a recent similar simulation of the monomer kink values of 3.7–10° were found.<sup>46</sup> The stronger kinking in this study is almost certainly due to the implicit nature of the membrane model. In the absence of an explicitly represented strongly ordered lipid phase, the helix can flex and bend more easily.

**Insertion Energy Profile from Simulations.** The fully flexible MC simulations of 1 × 10<sup>9</sup> MC steps are sufficiently long to yield converged insertion free energy landscapes from a direct population analysis. For both the capped and uncapped simulations with 2*L* = 30 Å, a two-dimensional population histogram was calculated as a function of the center-of-mass position along the membrane normal and the tilt angle. The negative logarithm of the histogram bins gives the overall solvation free energy profile of the system and is plotted in Figure 4. The free energies are relative to the lowest bin, which has been set to zero. A close similarity to the profiles shown in Figures 1 and 3 is evident and expected. Note that the profiles in Figure 4 can only extend over the conformational space that was physically sampled, while the rigid-body scan results above can plot the entire landscape—albeit for a fixed conformation. Figure 4 panel A reveals the uncapped peptide has thoroughly explored the TM inserted minimum at *z* = 4.5 Å, tilt = 16.6° and remains

strongly contained by large barriers, as already visible in Figure 1. The results for the capped peptide shown in Figure 4 panel B are very different. After spending considerable time sampling the TM bound state at *z* = 6.3 Å, tilt = 18.1°, the peptide overcomes the weak barrier (see also Figure 3) after ~500 × 10<sup>6</sup> MC steps and exits to the surface of the membrane. The small barrier height—caused by the lack of charged groups on the N-terminal side of the Vpu peptide—is only ~2 kcal/mol, even smaller than the estimate of ~6 kcal/mol from the rigid body scan.

**Folding Simulations.** The next step is to demonstrate that the implicit membrane model can predict the experimentally determined native state of Vpu in an ab initio protein folding simulation. For this, REMC simulations were run with 10 replicas for 1 × 10<sup>9</sup> MC steps each (see Methods), starting from completely extended conformations perpendicular to the membrane plane. The simulations were performed both for capped Vpu and for the uncapped system. Figure 5 shows the folding progress of the transmembrane system over the course of the simulations. Only the 318 K replica, the temperature closest to the NMR experiments, is shown. Both capped and uncapped Vpu fold into stable membrane spanning helices within the first ~400 × 10<sup>6</sup> MC steps. Replicas with higher temperatures contain a large amount of helical secondary structure but do not form stable helices. No beta structure is observed in any of the simulations. Once formed, the helix shows strong tilting and kinking. To quantify the similarity to the native state—the completely helical structure found in the NMR measurements,<sup>41</sup> we calculated the overall system helicity as it increases over the course of the simulation, and the results are shown in Figure 6. After a steady buildup of helical content, a plateau is reached after ~400 × 10<sup>6</sup> MC steps. The chain ends are

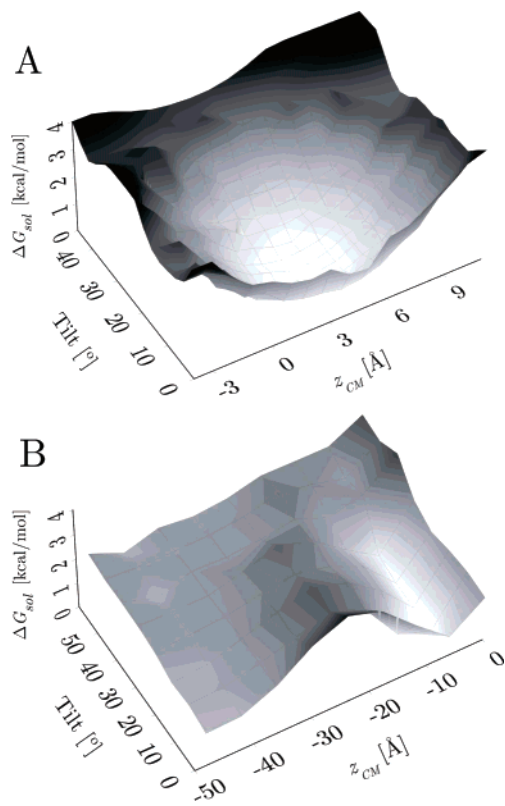


**Figure 4.** Free energy profile of Vpu as calculated from a population analysis for the fully flexible MC simulations in TM bound conformation.  $\Delta G$  is plotted as a function of the helix tilt and center-of-mass position along the membrane normal, and is the free energy relative to the lowest bin that has been set to zero. The uncapped system is shown in panel A, revealing a stable TM inserted minimum at  $z = 4.5$  Å, tilt =  $16.6^\circ$ , as found in the rigid-body scan (Figure 1). The capped system plotted in panel B shows the same TM minimum but is not stable and exits the TM state after  $500 \times 10^6$  MC steps. The weak barrier (see also Figure 3) is caused by the lack of charged groups on the N-terminal side of the Vpu peptide.

found to be flexible and mostly do not sample helical conformations.

The folding results are directly compared to the single fully flexible  $1 \times 10^9$  MC step simulations of Vpu starting from the helical TM conformation, and the helicity is plotted in the same Figure 6. For both the capped and uncapped peptide strong tilting and kinking is observed (see Tables 1 and 2), but the completely helical conformation remains intact during the runs, with  $78.5\% \pm 6.6\%$  helicity for the uncapped peptide and  $66.5\% \pm 2.3\%$  for the capped system. The lower helicity of the capped peptide is due to the more flexible chain termini. While the REMC folding run for the capped peptide reaches the same plateau in helicity as the reference native run, the helicity observed for the REMC folding run with the uncapped peptide is lower. This indicates a sampling problem of the more highly polar system, where partly helical structures present in the various replicas persist much longer due to charge–charge interactions than in the case of the capped system, where the complete helix quickly dominates. Such partly helical structures are swapped into the 318 K replica and thus contribute to the overall helicity. Contrary,

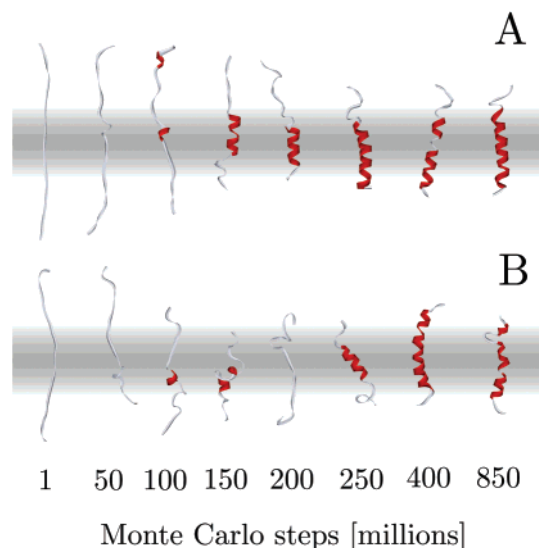


**Figure 5.** Transmembrane folding of Vpu for the 318 K replica of the REMC simulations, showing the capped system (panel A) and the uncapped system (panel B). Vpu folds into a stable membrane spanning helices within the first  $\sim 400 \times 10^6$  MC steps. Higher temperature replicas retain largely extended or coiled conformations (data not shown). It should be noted that the implicit membrane does not represent a hydrophobic slab but rather a Gaussian shaped hydrophobic zone, thus the 30 Å slabs shown are for reference only.

in the native TM state simulation of the uncapped peptide, partly helical conformations are not sampled at all. Overall, the results prove that the native state of Vpu can be accurately predicted after a relatively short MC simulation from a completely random conformation. The choice of the chain termini seems to not influence these results. This matches experimental observations that found the effect of terminal caps on the helicity of a designed TM bound peptide to be marginal.<sup>81</sup>

In order to investigate the role of the cutoff of the non-bonded interactions, an additional REMC run was performed with a complete evaluation of all nonbonded interactions (no cutoff), including the GB terms. In general, the GB model is ideal when truncating electrostatic interactions: The Coulomb term ( $E_{coul}$ ) plus the GB polarization term ( $\Delta G_{pol}$ ) for two largely separated atoms is simply a screened Coulomb interaction, weakened by  $\epsilon_{water}$ . Thus, the contribution of these far terms to the total nonbonded energy is much smaller than in vacuum electrostatics. However, for deeply buried atoms (e.g., atoms in the membrane interior), the resulting large Born radii will reduce their contribution to  $\Delta G_{pol}$  so much that cutoff artifacts of  $E_{coul}$  may still be significant.

The simulation was carried out identically to the folding simulations above. No significant deviation to the folding runs using a cutoff were detected. The buildup of helicity during the simulation is shown in Figure 5 and is almost the same as in the other runs. Thus we conclude that cutoff effects do not significantly influence the folding results.

**Vpu Channel Simulation.** Vpu polypeptides that contain the membrane spanning segment have ion-channel activity, and since Vpu forms single TM helices, this is achieved by

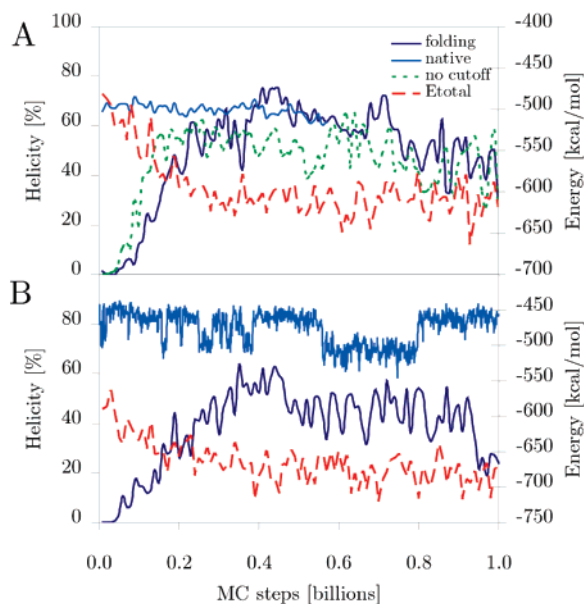


**Figure 6.** This graph shows the buildup of the helicity of Vpu for the 318 K replica during the folding runs of  $1 \times 10^9$  MC steps (left axis – solid lines) and the change of the total system energy (internal energy plus solvation free energy, right axis – dotted line). The helicity of the single simulations starting from the native helical TM inserted state is also shown in the same plot for comparison. Panel **A**: capped system. The two folding trajectories are with and without cutoffs, respectively. Panel **B**: uncapped peptide. In both cases, the complete TM helix forms in  $\sim 400 \times 10^6$  MC steps. Due to frequent replica swaps to only partly helical structures that contribute to the average, the helicity is lower in the REMC folding runs and fluctuates much more, indicating longer sampling is still required (i.e., not all replicas have folded). In the native MC runs, the helix remains completely stable, but the capped peptide exits the membrane after  $\sim 500 \times 10^6$  MC steps.

their oligomerization in lipid bilayers. The N-terminal TM domain of Vpu has been shown to form homo-oligomers both in vivo and in vitro.<sup>35</sup> Oligomeric Vpu has a cation-specific channel activity for which only the TM sequence is required.<sup>36–40</sup> The structure of the oligomer is not known, but a pentamer is thought most likely, as suggested by several simulation studies<sup>49–55</sup> and estimated from single-channel conductance measurements.<sup>52</sup> We set up the pentamer in the implicit membrane, using the structure proposed by Park et al.<sup>42</sup> (PDB code 1PI7), with the interfacial tryptophan residues facing the lipid environment. The missing residues (1–6, 26–30) of each chain were added with an  $\alpha$ -helical secondary structure. The MC simulation was run for  $240 \times 10^6$  steps without any constraints and without any cutoffs for the nonbonded interactions.

The pentamer remains stable throughout the simulation, as shown in Figure 7, with all five helices firmly interlocked at their hydrophobic segments. No displacement normal to the membrane plane is observed, and the pentamer remains in its inserted state, anchoring the tryptophan residues at the interface, the preferred location for this amino acid.<sup>73,74,82</sup> There is no loss of helical structure except at the chain ends, where a slight unwinding is observed (panel B). Panel C

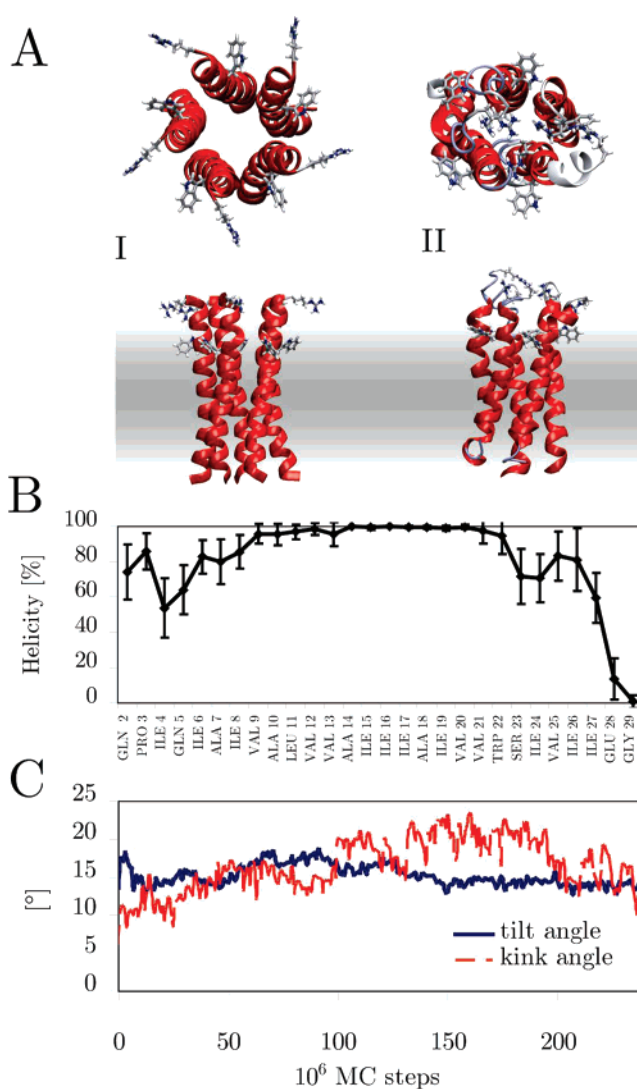


**Figure 7.** Vpu pentamer simulation. **A**: View from the top (C-terminal to N-terminal) and the side of the first (I) and the final structure (II) of the  $240 \times 10^6$  MC step simulation. **B**: average helicity per residue over the course of the simulation. **C**: average tilt and kink angle calculated over the center segment of the 5 monomers during the simulations.

shows the development of the tilt and kink angles averaged over the individual helices as a function of simulation time. The average tilt of  $15^\circ \pm 1.4^\circ$  is similar to the  $14.5^\circ$  reported by Cordes et al. in explicit lipid and solvent simulation,<sup>52</sup> while the average kink angle of  $16^\circ \pm 3.5^\circ$  is slightly smaller than the  $19.9^\circ$  obtained in that study. These values are smaller than those of the Vpu monomer, which can be explained by the thicker membrane environment and the fact that the helices are firmly bound to each other, preventing stronger tilting. For the same reason, there is less fluctuation in the tilt and kink angle throughout the run.

The loss of helical structure at the N-terminus, involving a proline residue, is only minor. Indeed it was observed experimentally that the tendency of proline to disrupt helical structures on membrane interfaces is weak.<sup>81</sup> Structural deviation from the helix is much more pronounced at the C-terminus and could be due to a limitation of the all-implicit model: In a fully explicit bilayer, this region corresponds

to the very dense lipid headgroup layer that would prevent significant helix perturbation. At present the implicit membrane model does not account for the polar nature of the lipid headgroup region, but it is in principle possible to add such a contribution. Interestingly, perturbation of helical structure was only sporadically observed in the monomer folding simulations, since the single helix can tilt more strongly to bury completely in the hydrophobic zone. In previously reported explicit MD pentamer simulations, significant structural change was not seen.<sup>49–55</sup> However, the limited sampling time (1–5 ns) of these simulations is much shorter than the extensive sampling achieved with the implicit membrane model. Cordes et al. speculate that the destabilization of the Vpu bundles at the C-terminal end are due to a EYR-motif, with the arginines covering the pore acting as a selectivity filter.<sup>52</sup> In our simulations, the even lower stability of the C-terminus is almost certainly caused by using a different mutant, with a glycine (EGR instead of EYR), but similar to the previous results, the arginines, with their flexible side chains, are found to point to the inside covering the pore throughout the simulations (Figure 7 panel A).

## Conclusion and Discussion

The secondary structure of the N-terminal transmembrane helix of Vpu is predicted in protein folding simulations using an implicit membrane model and all-atom representation of the protein. It forms a stable helix firmly inserted in the membrane, and the observed average tilt and kink angles closely match experimental results from NMR measurements. In addition, the experimentally observed increase of the helix tilt in membranes of decreasing hydrophobic thickness ('hydrophobic mismatch') is accurately reproduced. The results reveal the strength of the generalized Born implicit membrane model in capturing the essential membrane energetics through a polarization term and a hydrophobic burial term. The lack of explicit lipid and solvent molecules enables greatly accelerated sampling currently not achievable in explicit bilayer simulations. A simulation of a pentamer of the transmembrane Vpu helix reveals a stable channel, in agreement with previous MD simulation efforts.

Simulating the folding of small membrane bound polypeptides and oligomeric TM bundles in a completely implicit membrane model is challenging. To be useful for studying a wide range of peptides, such methods must essentially fulfill several requirements: (a) single TM or surface bound helices as well as integral membrane proteins must retain their experimentally observed structure (e.g., NMR data) despite being surrounded only by a continuum environment, (b) such stability must not be caused by the use of models and parameter sets that overly bias helical structures or by the use of artificial constraining potentials, (c) in order to justify the substantial simplifications entailed by an implicit representation of the membrane the model must be significantly faster than equivalent fully atomistic membrane simulations, enabling extensive conformational sampling that goes beyond simple rigid orientational scans, and (d) a wide range of experimental data must be reproduced, especially the experimentally determined partitioning free energy of polypeptides into both the membrane interfaces and the

membrane interior (biophysical and statistical hydrophobicity scales)<sup>70,83</sup> as well as the recent biological hydrophobicity scale determined by translocon mediated insertion.<sup>84</sup>

While the presented implicit membrane model performs well on these points, we have identified two key deficiencies that have yet to be overcome: The neglect of effects due to the complex lipid headgroup environment and the improper treatment of charged residues. In practical terms, this signifies that the interfacial regions of the membrane are poorly described, and some loss of defined secondary structure is observed in the segments of membrane bound peptides in this region. This will be especially problematic for simulating surface bound peptides (e.g., antimicrobials) and matching experimental partitioning free energy of unfolded polypeptides into membrane interfaces.<sup>85</sup> For charged residues, the GB model predicts a large desolvation penalty on moving into the hydrophobic region. In the biological scale of Hessa et al., the effect of the additional charge is almost non-existent: For example, the apparent free energy of insertion  $\Delta G_{\text{app}}^{\text{aa}}$  of an amino acid located at the center of a 19 residue TM helix is roughly equally unfavorable for glutamine (2.36) and glutamic acid (2.68),<sup>84</sup> whereas the burial penalty due to the additional full charge is large in the GB model. It would therefore be more appropriate to use variable protonation state models, where residues can be neutralized upon entering the membrane. Alternatively, White et al. suggests that the strong positional dependence of charged residues in the biological scale could be due to distorted bilayer states, where the headgroups are in contact with buried peptide charges, and the hydrophobic thickness is significantly reduced.<sup>86</sup> This is currently beyond the limits of the implicit membrane model.

The subtle energetic and entropic effects that can be neglected when representing the complex lipid bilayer environment implicitly are illustrated by a recently reported study of TM bundles in an implicit GB membrane by Bu et al.,<sup>22</sup> where predicting the correct native oligomerization state of several homo-oligomers was only partially achieved. A high population of non-native (as compared to the NMR structure) equilibrium structures were encountered at experimental temperatures. The authors used a cylindrical harmonic restraining potential to prevent the oligomers from disintegrating into individual helices drifting away from each other, enabling stability at the elevated temperatures used in the replica exchange runs. In our simulations, no restraining potential is used, with the Vpu pentamer remaining tightly packed throughout the simulation.

Ultimately, further improvement is required for a more accurate modeling of the polar lipid headgroup region of the membrane, which will involve additions to the implicit membrane that go beyond simple dielectric treatment. In addition, the inclusion of variable protonation state models is probably a good idea if sequences with many charged residues are studied. Such efforts are currently underway.

**Acknowledgment.** We are grateful to A. Di Nola for helpful discussions. J.P.U. is funded by an Emmy Noether fellowship of the German Research Foundation. M.B.U. is funded by an international fellowship of the Wellcome Trust.

## References

- (1) Biggin, P. C.; Sansom, M. S. Interactions of alpha-helices with lipid bilayers: a review of simulation studies. *Biophys. Chem.* **1999**, *76*, 161–183.
- (2) Forrest, L. R.; Sansom, M. S. P. Membrane simulations: bigger and better? *Curr. Opin. Struct. Biol.* **2000**, *10*, 174–181.
- (3) Domene, C.; Bond, P. J.; Sansom, M. S. P. Membrane protein simulations: Ion channels and bacterial outer membrane proteins. In *Protein Simulations*; Daggett, V., Ed.; Academic Press Inc.: San Diego, CA, 2003; Vol. 66, p 159+.
- (4) Nymeyer, H.; Woolf, T. B.; Garcia, A. E. Folding is not required for bilayer insertion: Replica exchange simulations of an alpha-helical peptide with an explicit lipid bilayer. *Proteins* **2005**, *59*, 783–790.
- (5) Braun, R.; Engelman, D. M.; Schulten, K. Molecular Dynamics Simulations of Micelle Formation around Dimeric Glycophorin A Transmembrane Helices. *Biophys. J.* **2004**, *87*, 754–63.
- (6) Bond, P. J.; Cuthbertson, J. M.; Deol, S. S.; Sansom, M. S. MD simulations of spontaneous membrane protein/detergent micelle formation. *J. Am. Chem. Soc.* **2004**, *126*, 15948–9.
- (7) Woolf, T. B.; Zuckerman, D. M.; Lu, N. D.; Jang, H. B. Tools for channels: moving towards molecular calculations of gating and permeation in ion channel biophysics. *J. Mol. Graph.* **2004**, *22*, 359–368.
- (8) Efremov, R. G.; Nolde, D. E.; Konshina, A. G.; Syrtcev, N. P.; Arseniev, A. S. Peptides and proteins in membranes: What can we learn via computer simulations? *Curr. Med. Chem.* **2004**, *11*, 2421–2442.
- (9) Feig, M.; Chocholoušová, J.; Tanizaki, S. Extending the horizon: towards the efficient modeling of large biomolecular complexes in atomic detail. *Theor. Chem. Acc.* **2006**, *116*, 194–205.
- (10) Born, M. Volumen und Hydratationswärme der Ionen. *Z. Phys.* **1920**, *1*, 45–48.
- (11) Still, W. C.; Tempczyk, A.; Hawley, R. C.; Hendrickson, T. Semianalytical Treatment of Solvation for Molecular Mechanics and Dynamics. *J. Am. Chem. Soc.* **1990**, *112*, 6127–6129.
- (12) Chowdhury, S.; Zhang, W.; Wu, C.; Xiong, G. M.; Duan, Y. Breaking non-native hydrophobic clusters is the rate-limiting step in the folding of an alanine-based peptide. *Biopolymers* **2003**, *68*, 63–75.
- (13) Jang, S.; Shin, S.; Pak, Y. Molecular dynamics study of peptides in implicit water: Ab initio folding of beta-hairpin, beta-sheet, and beta beta alpha- motif. *J. Am. Chem. Soc.* **2002**, *124*, 4976–4977.
- (14) Simmerling, C.; Strockbine, B.; Roitberg, A. E. All-atom structure prediction and folding simulations of a stable protein. *J. Am. Chem. Soc.* **2002**, *124*, 11258–11259.
- (15) Snow, C. D.; Nguyen, N.; Pande, V. S.; Gruebele, M. Absolute comparison of simulated and experimental protein-folding dynamics. *Nature* **2002**, *420*, 102–106.
- (16) Ulmschneider, J. P.; Jorgensen, W. L. Polypeptide folding using Monte Carlo sampling, concerted rotation, and continuum solvation. *J. Am. Chem. Soc.* **2004**, *126*, 1849–1857.
- (17) Spassov, V. Z.; Yan, L.; Szalma, S. Introducing an implicit membrane in generalized Born/solvent accessibility continuum solvent models. *J. Phys. Chem. B* **2002**, *106*, 8726–8738.
- (18) Im, W.; Feig, M.; Brooks, C. L., III. An implicit membrane generalized born theory for the study of structure, stability, and interactions of membrane proteins. *Biophys. J.* **2003**, *85*, 2900–2918.
- (19) Tanizaki, S.; Feig, M. A generalized Born formalism for heterogeneous dielectric environments: application to the implicit modeling of biological membranes. *J. Chem. Phys.* **2005**, *122*, 124706.
- (20) Tanizaki, S.; Feig, M. Molecular Dynamics Simulations of Large Integral Membrane Proteins with an Implicit Membrane Model. *J. Phys. Chem. B* **2006**, *110*, 548–556.
- (21) Ulmschneider, M. B.; Ulmschneider, J. P.; Sansom, M. S. P.; Di Nola, A. A generalized Born implicit membrane representation compared to experimental insertion free energies. *Biophys. J.* **2007**, *92*, 2338–2349.
- (22) Bu, L.; Im, W.; Brooks, C. L., III. Membrane Assembly of Simple Helix Homo-Oligomers Studied via Molecular Dynamics Simulations. *Biophys. J.* **2007**, *92*, 854–863.
- (23) Im, W.; Brooks, C. L. Interfacial folding and membrane insertion of designed peptides studied by molecular dynamics simulations. *Proc. Natl. Acad. Sci.* **2005**, *102*, 6771–6776.
- (24) Im, W.; Brooks, C. L., III. De novo Folding of Membrane Proteins: An Exploration of the Structure and NMR Properties of the fd Coat Protein. *J. Mol. Biol.* **2004**, *337*, 513–519.
- (25) Lee, J.; Im, W. Implementation and application of helix-helix distance and crossing angle restraint potentials. *J. Comput. Chem.* **2007**, *28*, 669–680.
- (26) Im, W.; Chen, J. H.; Brooks, C. L. Peptide and protein folding and conformational equilibria: Theoretical treatment of electrostatics and hydrogen bonding with implicit solvent models. In *Peptide Solvation and H-Bonds*; Baldwin, R., Baker, D., Eds.; Elsevier Academic Press Inc.: San Diego, CA, 2006; Vol. 72, pp 173–198.
- (27) Ulmschneider, J. P.; Ulmschneider, M. B.; Di Nola, A. Monte Carlo folding of trans-membrane helical peptides in an implicit generalized Born membrane. *Proteins* **2007**, in press.
- (28) Cohen, E. A.; Terwilliger, E. F.; Sodroski, J. G.; Haseltine, W. A. Identification of a Protein Encoded by the Vpu Gene of Hiv-1. *Nature* **1988**, *334*, 532–534.
- (29) Strebel, K.; Klimkait, T.; Martin, M. A. A Novel Gene of Hiv-1, Vpu, and Its 16-Kilodalton Product. *Science* **1988**, *241*, 1221–1223.
- (30) Marassi, F. M.; Ma, C.; Gratkowski, H.; Straus, S. K.; Strebel, K.; Oblatt-Montal, M.; Montal, M.; Opella, S. J. Correlation of the structural and functional domains in the membrane protein Vpu from HIV-1. *Proc. Natl. Acad. Sci.* **1999**, *96*, 14336–14341.
- (31) Willey, R. L.; Maldarelli, F.; Martin, M. A.; Strebel, K. Human-immunodeficiency-virus type-1 Vpu protein regulates the formation of intracellular Gp160-Cd4 complexes. *J. Virol.* **1992**, *66*, 226–234.
- (32) Levesque, K.; Finzi, A.; Binette, J.; Cohen, E. A. Role of CD4 receptor down-regulation during HIV-1 infection. *Curr. HIV Res.* **2004**, *2*, 51–59.

- (33) Klimkait, T.; Strebel, K.; Hoggan, M. D.; Martin, M. A.; Orenstein, J. M. The human immunodeficiency virus type 1-specific protein Vpu is required for efficient virus maturation and release. *J. Virol.* **1990**, *64*, 621–629.
- (34) Strebel, K.; Klimkait, T.; Maldarelli, F.; Martin, M. A. Molecular and biochemical analyses of human immunodeficiency virus type-1 Vpu protein. *J. Virol.* **1989**, *63*, 3784–3791.
- (35) Maldarelli, F.; Chen, M. Y.; Willey, R. L.; Strebel, K. Human-immunodeficiency-virus type-1 Vpu protein is an oligomeric type-I integral membrane-protein. *J. Virol.* **1993**, *67*, 5056–5061.
- (36) Ma, C.; Marassi, F. M.; Jones, D. H.; Straus, S. K.; Bour, S.; Strebel, K.; Schubert, U.; Oblatt-Montal, M.; Montal, M.; Opella, S. J. Expression, purification, and activities of full-length and truncated versions of the integral membrane protein Vpu, from HIV-1. *Protein Sci.* **2002**, *11*, 546–557.
- (37) Kochendoerfer, G. G.; Jones, D. H.; Lee, S.; Oblatt-Montal, M.; Opella, S. J.; Montal, M. Functional characterization and NMR spectroscopy on full-length Vpu from HIV-1 prepared by total chemical synthesis. *J. Am. Chem. Soc.* **2004**, *126*, 2439–46.
- (38) Schubert, U.; FerrerMontiel, A. V.; OblattMontal, M.; Henklein, P.; Strebel, K.; Montal, M. Identification of an ion channel activity of the Vpu transmembrane domain and its involvement in the regulation of virus release from HIV-1-infected cells. *FEBS Lett.* **1996**, *398*, 12–18.
- (39) Ewart, G. D.; Sutherland, T.; Gage, P. W.; Cox, G. B. The Vpu protein of human immunodeficiency virus type 1 forms cation-selective ion channels. *J. Virol.* **1996**, *70*, 7108–7115.
- (40) Romer, W.; Lam, Y. H.; Fischer, D.; Watts, A.; Fischer, W. B.; Goring, P.; Wehrspohn, R. B.; Gosele, U.; Steinem, C. Channel activity of a viral transmembrane peptide in micro-BLMs: Vpu(1-32) from HIV-1. *J. Am. Chem. Soc.* **2004**, *126*, 16267–16274.
- (41) Park, S. H.; Mrse, A. A.; Nevzorov, A. A.; Mesleh, M. F.; Oblatt-Montal, M.; Montal, M.; Opella, S. J. Three-dimensional structure of the channel-forming trans-membrane domain of virus protein “u” (Vpu) from HIV-1. *J. Mol. Biol.* **2003**, *333*, 409–24.
- (42) Park, S. H.; De Angelis, A. A.; Nevzorov, A. A.; Wu, C. H.; Opella, S. J. Three-dimensional Structure of the Transmembrane Domain of Vpu from HIV-1 in Aligned Phospholipid Bicelles. *Biophys. J.* **2006**, *91*, 3032–3042.
- (43) Park, S. H.; Opella, S. J. Tilt angle of a trans-membrane helix is determined by hydrophobic mismatch. *J. Mol. Biol.* **2005**, *350*, 310–318.
- (44) Sharpe, S.; Yau, W. M.; Tycko, R. Structure and dynamics of the HIV-1 Vpu transmembrane domain revealed by solid-state NMR with magic-angle spinning. *Biochemistry* **2006**, *45*, 918–33.
- (45) Kukol, A.; Arkin, I. T. Vpu transmembrane peptide structure obtained by site-specific fourier transform infrared dichroism and global molecular dynamics searching. *Biophys. J.* **1999**, *77*, 1594–601.
- (46) Lemaitre, V.; Willbold, D.; Watts, A.; Fischer, W. B. Full length Vpu from HIV-1: Combining molecular dynamics simulations with NMR spectroscopy. *J. Biomol. Struct. Dyn.* **2006**, *23*, 485–496.
- (47) Sramala, I.; Lemaitre, V.; Faraldo-Gomez, J. D.; Vincent, S.; Watts, A.; Fischer, W. B. Molecular dynamics simulations on the first two helices of Vpu from HIV-1. *Biophys. J.* **2003**, *84*, 3276–3284.
- (48) Sun, F. Molecular dynamics simulation of human immunodeficiency virus protein U (Vpu) in lipid/water Langmuir monolayer. *J. Mol. Model.* **2003**, *9*, 114–123.
- (49) Grice, A. L.; Kerr, I. D.; Sansom, M. S. P. Ion channels formed by HIV-1 Vpu: A modelling and simulation study. *FEBS Lett.* **1997**, *405*, 299–304.
- (50) Moore, P. B.; Zhong, Q. F.; Husslein, T.; Klein, M. L. Simulation of the HIV-1 Vpu transmembrane domain as a pentameric bundle. *FEBS Lett.* **1998**, *431*, 143–148.
- (51) Cordes, F. S.; Kukol, A.; Forrest, L. R.; Arkin, I. T.; Sansom, M. S. P.; Fischer, W. B. The structure of the HIV-1 Vpu ion channel: modelling and simulation studies. *Biochim. Biophys. Acta* **2001**, *1512*, 291–298.
- (52) Cordes, F. S.; Tustian, A. D.; Sansom, M. S. P.; Watts, A.; Fischer, W. B. Bundles consisting of extended transmembrane segments of Vpu from HIV-1: Computer simulations and conductance measurements. *Biochemistry* **2002**, *41*, 7359–7365.
- (53) Lopez, C. F.; Montal, M.; Blasie, J. K.; Klein, M. L.; Moore, P. B. Molecular dynamics investigation of membrane-bound bundles of the channel-forming transmembrane domain of viral protein U from the human immunodeficiency virus HIV-1. *Biophys. J.* **2002**, *83*, 1259–1267.
- (54) Kim, C. G.; Lemaitre, V.; Watts, A.; Fischer, W. B. Drug-protein interaction with Vpu from HIV-1: proposing binding sites for amiloride and one of its derivatives. *Anal. Bioanal. Chem.* **2006**, *386*, 2213–2217.
- (55) Lemaitre, V.; Ali, R.; Kim, C. G.; Watts, A.; Fischer, W. B. Interaction of amiloride and one of its derivatives with Vpu from HIV-1: a molecular dynamics simulation. *FEBS Lett.* **2004**, *563*, 75–81.
- (56) Bond, P. J.; Holyoake, J.; Ivetac, A.; Khalid, S.; Sansom, M. S. P. Coarse-grained molecular dynamics simulations of membrane proteins and peptides. *J. Struct. Biol.* **2007**, *157*, 593–605.
- (57) Qiu, D.; Shenkin, P. S.; Hollinger, F. P.; Still, W. C. The GB/SA continuum model for solvation. A fast analytical method for the calculation of approximate Born radii. *J. Phys. Chem. A* **1997**, *101*, 3005–3014.
- (58) Gallicchio, E.; Levy, R. M. AGBNP: An analytic implicit solvent model suitable for molecular dynamics simulations and high-resolution modeling. *J. Comput. Chem.* **2004**, *25*, 479–499.
- (59) Im, W.; Lee, M. S.; Charles, L.; Brooks, I. Generalized born model with a simple smoothing function. *J. Comput. Chem.* **2003**, *24*, 1691–1702.
- (60) Jorgensen, W. L.; Ulmschneider, J. P.; Tirado-Rives, J. Free energies of hydration from a generalized Born model and an ALL-atom force field. *J. Phys. Chem. B* **2004**, *108*, 16264–16270.
- (61) Parsegian, A. Energy of an Ion crossing a Low Dielectric Membrane: Solutions to Four Relevant Electrostatic Problems. *Nature* **1969**, *221*, 844–846.
- (62) Schaefer, M.; Bartels, C.; Karplus, M. Solution conformations and thermodynamics of structured peptides: molecular dynamics simulation with an implicit solvation model. *J. Mol. Biol.* **1998**, *284*, 835–48.

- (63) Radzicka, A.; Wolfenden, R. Comparing the Polarities of the Amino-Acids - Side-Chain Distribution Coefficients between the Vapor-Phase, Cyclohexane, 1-Octanol, and Neutral Aqueous-Solution. *Biochemistry* **1988**, *27*, 1664–1670.
- (64) Ulmschneider, J. P.; Jorgensen, W. L. Monte Carlo backbone sampling for polypeptides with variable bond angles and dihedral angles using concerted rotations and a Gaussian bias. *J. Chem. Phys.* **2003**, *118*, 4261–4271.
- (65) Jorgensen, W. L.; Maxwell, D. S.; Tirado-Rives, J. Development and testing of the OPLS all-atom force field on conformational energetics and properties of organic liquids. *J. Am. Chem. Soc.* **1996**, *118*, 11225–11236.
- (66) Ulmschneider, J. P.; Jorgensen, W. L. Monte Carlo backbone sampling for nucleic acids using concerted rotations including variable bond angles. *J. Phys. Chem. B* **2004**, *108*, 16883–16892.
- (67) Ulmschneider, J. P.; Ulmschneider, M. B.; Di Nola, A. Monte Carlo vs Molecular Dynamics for All-Atom Polypeptide Folding Simulations. *J. Phys. Chem. B* **2006**, *110*, 16733–42.
- (68) Sugita, Y.; Okamoto, Y. Replica-exchange molecular dynamics method for protein folding. *Chem. Phys. Lett.* **1999**, *314*, 141–151.
- (69) Earl, D. J.; Deem, M. W. Parallel tempering: Theory, applications, and new perspectives. *Phys. Chem. Chem. Phys.* **2005**, *7*, 3910–3916.
- (70) Ulmschneider, M. B.; Sansom, M. S.; Di Nola, A. Properties of integral membrane protein structures: derivation of an implicit membrane potential. *Proteins* **2005**, *59*, 252–65.
- (71) Ulmschneider, M. B.; Sansom, M. S.; Di Nola, A. Evaluating tilt angles of membrane-associated helices: comparison of computational and NMR techniques. *Biophys. J.* **2006**, *90*, 1650–60.
- (72) von Heijne, G. Principles of membrane protein assembly and structure. *Prog. Biophys. Mol. Biol.* **1997**, *66*, 113–139.
- (73) Ulmschneider, M. B.; Sansom, M. S. P. Amino acid distributions in integral membrane protein structures. *Biochim. Biophys. Acta-Biomembr.* **2001**, *1512*, 1–14.
- (74) Yau, W. M.; Wimley, W. C.; Gawrisch, K.; White, S. H. The preference of tryptophan for membrane interfaces. *Biochemistry* **1998**, *37*, 14713–14718.
- (75) Strandberg, E.; Morein, S.; Rijkers, D. T.; Liskamp, R. M.; van der Wel, P. C.; Killian, J. A. Lipid dependence of membrane anchoring properties and snorkeling behavior of aromatic and charged residues in transmembrane peptides. *Biochemistry* **2002**, *41*, 7190–7198.
- (76) de Planque, M. R.; Kruijtzter, J. A.; Liskamp, R. M.; Marsh, D.; Greathouse, D. V.; Koeppe, R. E., II; de Kruijff, B.; Killian, J. A. Different membrane anchoring positions of tryptophan and lysine in synthetic transmembrane alpha-helical peptides. *J. Biol. Chem.* **1999**, *274*, 20839–20846.
- (77) White, S. H.; von Heijne, G. Transmembrane helices before, during, and after insertion. *Curr. Opin. Struct. Biol.* **2005**, *15*, 378–386.
- (78) Killian, J. A.; Salemink, I.; de Planque, M. R.; Lindblom, G.; Koeppe, R. E., II; Greathouse, D. V. Induction of nonbilayer structures in diacylphosphatidylcholine model membranes by transmembrane alpha-helical peptides: importance of hydrophobic mismatch and proposed role of tryptophans. *Biochemistry* **1996**, *35*, 1037–1045.
- (79) White, S. H.; Wimley, W. C. Hydrophobic interactions of peptides with membrane interfaces. *Biochim. Biophys. Acta* **1998**, *1376*, 339–52.
- (80) Duong-Ly, K. C.; Nanda, V.; Degrad, W. F.; Howard, K. P. The conformation of the pore region of the M2 proton channel depends on lipid bilayer environment. *Protein Sci.* **2005**, *14*, 856–861.
- (81) Ladokhin, A. S.; White, S. H. Interfacial Folding and Membrane Insertion of a Designed Helical Peptide. *Biochemistry* **2004**, *43*, 5782–5791.
- (82) de Planque, M. R.; Bonev, B. B.; Demmers, J. A.; Greathouse, D. V.; Koeppe, R. E., II; Separovic, F.; Watts, A.; Killian, J. A. Interfacial anchor properties of tryptophan residues in transmembrane peptides can dominate over hydrophobic matching effects in peptide-lipid interactions. *Biochemistry* **2003**, *42*, 5341–5348.
- (83) Wimley, W. C.; Creamer, T. P.; White, S. H. Solvation energies of amino acid side chains and backbone in a family of host-guest pentapeptides. *Biochemistry* **1996**, *35*, 5109–24.
- (84) Hessa, T.; Kim, H.; Bihlmaier, K.; Lundin, C.; Boekel, J.; Andersson, H.; Nilsson, I.; White, S. H.; von Heijne, G. Recognition of transmembrane helices by the endoplasmic reticulum translocon. *Nature* **2005**, *433*, 377–81.
- (85) Hristova, K.; White, S. H. An Experiment-Based Algorithm for Predicting the Partitioning of Unfolded Peptides into Phosphatidylcholine Bilayer Interfaces. *Biochemistry* **2005**, *44*, 12614–12619.
- (86) White, S. H.; von Heijne, G. Do protein-lipid interactions determine the recognition of transmembrane helices at the ER translocon? *Biochem. Soc. Trans.* **2005**, *33*, 1012–5.

CT700103K